RSC Advances

PAPER

View Article Online
View Journal | View Issue

Cite this: *RSC Adv.*, 2022, **12**, 30030

High lignin-containing nanocelluloses prepared *via* TEMPO-mediated oxidation and polyethylenimine functionalization for antioxidant and antibacterial applications†

Yisheng Sun,[a] Hanwen Zhang,[a] Qianwei Li,[a] Bongkosh Vardhanabhuti[b] and Caixia Wan *[a]

Lignin-containing nanocelluloses (LNCs) have attracted tremendous research interest in recent years due to less complex extraction processes and more abundant functionality compared to lignin-free nanocelluloses. On the other hand, traditional defibrillation primarily based on bleached pulp would not be readily applied to lignin-containing pulps due to their complex compositions. This study was focused on LNC extraction from lignin-containing pulp *via* 2,2,6,6-tetramethylpiperidine-1-oxyl radical (TEMPO)-mediated oxidation. Three types of switchgrass pulp with varying composition were prepared using different acid-catalyzed pretreatments. The pulps contained as high as 45.76% lignin but minor/no hemicellulose, corresponding to up to 23.72% lignin removal and 63.75–100% hemicellulose removal. TEMPO-mediated oxidation yielded 52.9–81.9% LNCs from respective pulps. The as-produced LNCs possessed aspect ratios as high as 416.5, and carboxyl contents of 0.442–0.743 mmol g^{-1} along with ζ-potential of −50.4 to −38.3 mV. The TEMPO-oxidized LNCs were further modified by polyethylenimine (PEI), which endowed the LNCs with positive charges plus antioxidant and antibacterial activities. Specifically, the PEI-modified LNCs almost fully scavenged 2,2′-azino-bis-3-ethylbenzthiazoline-6-sulphonic acid (ABTS) radicals at 50 mg L^{-1} and suppressed the growth of Gram-positive *Staphylococcus aureus* at 250 μg mL^{-1}.

Received 5th July 2022
Accepted 27th September 2022

DOI: 10.1039/d2ra04152a

rsc.li/rsc-advances

1. Introduction

Cellulose is the most abundant biopolymer on earth and provides a platform substrate for manufacturing of biofuels, products, and materials.[1–3] One example is extraction of nanocellulose from cellulose-rich biomass. Nanocellulose, which refers to cellulose with diameter below 100 nm, can serve as a platform nanomaterial given its high aspect ratios and surface areas, abundant functional groups, and high mechanical strength.[4–9] Therefore, nanocellulose has been explored as nanofillers for mechanical reinforcement of composites, nanocarriers for drug delivery, rheological modifiers in 3D-printable materials, and so forth.[10–12] Nanocellulose-based materials can also offer high performance in biological and biomedical applications due to their biocompatibility and low cytotoxicity.[13–15]

Nanocellulose production from lignocellulosic biomass typically involves a pretreatment step to disrupt recalcitrant lignocellulose complexes (LCCs) and a nanofibrillation step to further break down cellulose fibrils to nanoscale.[16–19] LCCs are a highly polymerized matrix where linear cellulose microfibrils with high crystallinity are sheathed by branched, covalently linked hemicellulose and lignin. Such structures provide plant mechanical strength and also prevent chemical and microbial attacks to plant cell walls.[20] The presence of lignin creates major barriers to disintegration of cellulose microfibrils by biological or chemical means.[21] Thus, bleached pulp, with lignin being fully removed, is vastly utilized in traditional nanocellulose production. On the other hand, more research efforts have recently been made to manufacture lignin-containing nanocelluloses (LNCs). Since extensive delignification is not a requirement, LNC manufacturing reduces process complexity, saves energy inputs and chemical uses, and minimizes generation of waste streams compared to nanocellulose extraction using bleached pulp.[22] Furthermore, LNCs have shown unique properties such as hydrophobicity, UV-blocking, antioxidant, and antimicrobial properties.[23,24] The processing advantages and attributes of LNCs may adapt such nanomaterials to

[a]*Department of Biomedical, Biological, and Chemical Engineering, University of Missouri, Columbia, Missouri 65211, USA. E-mail: wanca@missouri.edu; Tel: +1 573 884 7882*

[b]*Division of Food, Nutrition & Exercise Sciences, University of Missouri, Columbia, Missouri 65211, USA*

† Electronic supplementary information (ESI) available. See https://doi.org/10.1039/d2ra04152a

various cellulose-rich biomass feedstocks and downstream applications.

Currently, LNC production mainly involves mechanical and chemical nanofibrillation, mostly adopted from lignin-free nanocellulose processing.[22] Mechanical nanofibrillation relies on mechanical shearing forces and is generally less sensitive to pulp compositions, while chemical reactions can be more influenced by the presence of lignin in cellulose pulp. Compared to mechanical nanofibrillation, chemical method can lead to nanocellulose with more desired attributes, such as smaller sizes, higher crystallinity, and modified functional groups.[25–27] However, due to the presence of lignin, the performances of traditional chemical nanofibrillation reactions may be compromised, and thus have not been systematically studied so far. Among chemical nanofibrillation reactions, 2,2,6,6-tetramethylpiperidine-1-oxyl radical (TEMPO)-mediated oxidation possesses uniqueness in that it produces nanocelluloses with small diameters of a few nanometers but with aspect ratios as high as hundreds.[17] The reaction is also an important technique to graft carboxyl groups onto the surface of nanocelluloses, which endows them with potential for further functionalization or cross-linking.[28,29] Wen and colleagues reported an efficient TEMPO-mediated LNC production using an alkaline peroxide-pretreated pulp,[30] but studies in this area are still limited and far from systematic. Particularly, pulps from different pretreatments may affect TEMPO-mediated oxidation differently and are therefore worth investigating.

The carboxyl groups grafted by TEMPO-mediated oxidation can make nanocellulose more favorable for surface modifications and functionalization. One approach for surface modifications is based on the reaction between carboxyl and amino groups. Polyethylenimine (PEI) is a type of linear or branched polymers rich in amino groups and positively charged after protonation. Nanomaterials containing PEIs are extensively explored in biological and medical applications such as antimicrobial, vaccine, and drug delivery due to their high affinity to negatively charged cell membranes.[31,32] PEI-modification could endow nanocelluloses with new functions, such as antioxidant and antimicrobial properties.[33,34] Highly branched PEI is often incorporated in hydrogel materials as a cross linker or thickener.[35,36] However, how such new functions are incorporated into LNCs has yet to be investigated especially from the perspective of lignin co-existing with nanocellulose.

The objective of this work was to study TEMPO-mediated oxidation of the pulps resulting from acid-catalyzed pretreatments, and further characterize the properties and functions of the pristine and PEI-modified LNCs. Three acid-catalyzed pretreatments, including hydrothermal, dilute acid, and choline chloride: oxalic acid deep eutectic solvent (DES) pretreatments, were used to pretreat raw switchgrass, and the as-produced pulps were utilized as the substrates in TEMPO-mediated oxidation. Properties of as-produced LNCs, such as composition, morphology, and surface chemistry, were characterized to understand the effects of pretreatment and TEMPO oxidation. The potential of TEMPO-oxidized LNCs for functionalization was demonstrated by surface modification with polyethylenimine (PEI), and the properties of PEI-modified LNCs were investigated to understand the role of lignin in antioxidant and antibacterial activities.

2. Materials and methods

2.1. Materials

Switchgrass was collected from the South Farm at University of Missouri in Columbia, Missouri, USA. It was air-dried, ground through 2 mm screen, and stored in an airtight container prior to use. Microcrystalline cellulose (Avicel PH-101) was purchase from Sigma-Aldrich (St Louis, MO, USA) and used as received. All the other chemicals were purchased from Fisher Scientific (Hampton, NH, USA) at least in ACS reagent grade (purity $\geq$ 95%) and used as received.

2.2. Pretreatment

For hydrothermal pretreatment (denoted as HT), 5 g of dry switchgrass was mixed with 50 mL of deionized (DI) water and reacted at 220 °C for 5 min and 180 °C for 30 min in a 100 mL Parr reactor. After cooling the reactor in air to 50 °C, the pulp was collected by vacuum filtration and further washed with DI water until the pH reached neutral. The washed pulp, denoted as HT180 and HT220 for the respective pretreatment temperature at 180 and 220 °C, was air dried and then stored in an airtight container prior to use. Dilute acid pretreatment (denoted as DA) was conducted by mixing 2.5 g of dry switchgrass with 50 mL of 2 wt% sulfuric acid in the Parr reactor followed by the reaction at 120 °C for 1 h. The pulp was collected and washed until its pH was neutral. The DES pretreatment was conducted using choline chloride: oxalic acid (denoted as OA). OA was prepared by mixing choline chloride and anhydrous oxalic acid by a 1 : 1 molar ratio at 80 °C with continuous magnetic stirring at 300 rpm until a clear liquid was obtained. The mixture containing 5 g of dry switchgrass and 100 g of OA was then reacted for 1 h at 100 °C in a preheated oil bath with continuous magnetic stirring at 300 rpm. After reaction, the pulp was cooled and collected by vacuum filtration and further washed with DI water to reach neutral.

2.3. TEMPO-mediated oxidation

The pulps was extracted for LNCs *via* TEMPO-mediated oxidation following the method previously reported.[37] A pulp suspension was first made by dispersing 1 g of pulp in 100 g of DI water followed by ultrasonication with a Branson 450 sonifier at 20 kHz and 1.2 W mL^{-1} for 10 min. Next, 0.1 g of sodium bromide and 15.3 mg of TEMPO were added to the suspension. After adjusting the pH to 10 using 1.0 N NaOH solution, sodium hypochlorite (NaClO) was manually dropwise added in a total amount of 5.13 g to trigger and continue the reaction. The pH was kept at 9.95–10.05 by adding NaClO or NaOH. The reaction ended when the pH remained constant at 10 without further addition of NaOH and was then quenched by adding 5 mL of 95% ethanol. LNCs from the reaction were thoroughly washed by dialysis in DI water bath until a constant conductivity of dialysate close to that of DI water was achieved. The suspensions were further ultrasonicated at 20 kHz and 1.2 W mL^{-1} for

15 min, and then passed through a 125 μm screen to remove large particles and aggregates. Each LNC sample was labeled by suffixing "-LNC" after its respective pulp, *e.g.*, HT220-LNC referred to the LNC sample produced from HT220 pulp. A lignin-free nanocellulose control sample was also prepared by processing Avicel PH-101 through the same procedure for TEMPO-oxidation followed by ultrasonication as described above. The control sample was labeled as cellulose nanofiber (CNF).

2.4. PEI modification

LNCs and CNFs were functionalized *via* surface modification with branched PEI (Sigma-Aldrich; Mn, ~60 000; primary : secondary : tertiary amines, 1 : 2 : 1). Briefly, the nanocellulose suspensions were adjusted to 0.3 wt% consistency, and 0.24 g of *N*-hydroxysuccinimide (NHS), 0.45 g of 1-ethyl-3-(3-dimethylaminopropyl)carbodiimide (EDC), and 4 g of PEI were added to the suspensions at the pH 7 with magnetic stirring at 300 rpm following the method previously reported with slight modification.[9] The reaction continued for 24 h at room temperature. Thereafter, the suspensions were transferred to dialysis tubing and washed in DI water until a constant conductivity of dialysate close to that of DI water was achieved. The modified samples were labeled by suffixing "-PEI" to the LNC samples, *e.g.*, HT220-LNC-PEI referred to the PEI-modified HT220-LNC.

2.5. Characterization

The solid recovery and yields of pretreated pulps and LNCs were calculated based on mass of pulps over raw switchgrass and mass of LNCs over pulps, respectively. The compositions of pulps and LNCs were analyzed following the NREL protocol.[38] Briefly, the samples went through a two-stage acid hydrolysis, first by 72 wt% sulfuric acid at 30 °C for 1 h and then by 4 wt% acid at 121 °C for 1 h at the second stage. After the hydrolysis, monomeric sugars were analyzed by an Agilent 1100 HPLC system equipped with a Bio-Rad Aminex HPX-87H$^+$ column and reflective index detector. Briefly, the hydrolysates were filtrated through 0.45 μm nylon syringe filter and analyzed using HPLC (Agilent 1200 series, Agilent Technologies, Palo Alto, USA). The mobile phase was 5 mM H_2SO_4 solution, eluting at 0.6 mL min^{-1}, and the temperatures of column and detector temperatures were at 65 and 40 °C, respectively. Spectrophotometric and gravimetric methods were used to determine acid-soluble lignin and Klason lignin, respectively. Carboxyl groups on LNCs were determined by a conductometric titration method and the conductivity was measured by a Hanna HI-5522 conductivity meter.[39,40] LNC suspensions were first adjusted to 20 g with 0.05 wt% consistency. Fifty microliters of NaCl (1.0 M) and 10 μL HCl (1.0 M) were subsequently added to the suspensions to increase their conductivity to 500–1000 μS cm^{-1} and reduce the pH to 3–4. The suspensions were then gradually titrated by 40 mM NaOH until the conductivity increased and reached a constant rate and the final pH turned 9 or higher. The titration plot showed three phases depending on the dominant charge carriers in the suspensions – strong acid, strong alkali, and a transition phase in between, which was determined by linear regression. Carboxyl contents were calculated based on the amount of NaOH consumed in the transition phase by LNCs in suspensions. Thermal stabilities of samples were characterized by an SDT-Q600 thermogravimetric analyzer (TGA). For analysis, each sample was heated from 20 to 800 °C at a rate of 20 °C min^{-1} under N_2 flow (20 mL min^{-1}).

The size distribution of nanocellulose samples were determined by atomic force microscope (AFM) and Gwyddion software. The diluted LNC suspension (10 μL, 0.001–0.005 wt%) was evenly spread on a 2.5 × 2.5 cm^2 mica substrate attached on a glass slide. After drying at 40 °C in a convection oven, the samples were scanned by an Asylum MFP-3D-BIO AFM (Santa Barbara, CA) equipped with a silicon nitride probe in contact mode. Hydrodynamic diameter and ζ-potential were characterized by a Malvern Zetasizer (Malvern Instruments Ltd, GB). The diluted LNC suspensions (0.02 wt% consistency, pH 5.5–7.0) were loaded in customized cells and scanned. The dispersant was set as water and the refractive index of LNC was 1.61.[41] X-ray diffraction (XRD) was conducted with a Bruker SMART CCD system. Air-dried LNC samples were scanned at 0.02° per step from 10° to 40°. The crystallinity index (CrI) of each LNC sample was determined by the maximum intensity of (200) peak (I_{200}) and the minimum intensity of amorphous cellulose (I_{AM}) at the valley around 18°: $\mathrm{CrI} = (I_{200} - I_{AM})/I_{200} \times 100\%$.[42] Attenuated total reflectance Fourier transform infrared spectroscopy (ATR-FTIR) was conducted using a Nicolet 4700 FTIR spectrometer (Thermo Electron Corp., Waltham, MA) equipped with a germanium crystal surface. All the samples were scanned through 400 to 4000 cm^{-1} at 4 cm^{-1} per step. Rheological properties of PEI-modified nanocelluloses were determined by an MCR 302 rheometer (Anton Paar, Graz, Austria) using a parallel-plate setting in a diameter of 25 mm and a minimum distance of 1 mm. PEI-modified nanocelluloses were concentrated by water evaporation at 50 °C to hydrogel with 12 wt% consistency and their viscosities were measured over a shear rate increasing from 0.1 to 1000 rad s^{-1} at 25 °C. Micromorphology of PEI-modified nanocellulose gels was inspected by scanning electron microscope (SEM). Briefly, CNF-PEI and HT220-LNC-PEI hydrogels were freeze-dried using a 4.5 L benchtop lyophilizer (Labconco Corp., MO), and the cross-sections of the freeze-dried gels were imaged by an FEI Quanta 600F Environmental SEM at 5 kV after 10 nm-Pt sputtering. Quantification of primary amino (–NH_2) functional groups in PEI-modified nanocelluloses followed a colorimetric method using 4-nitrobenzaldehyde as described in the ESI.†[43]

Antioxidant activities of nanocelluloses were determined by their radical scavenging activities against 1,1-diphenyl-2-picrylhydrazyl (DPPH) and 2,2′-azino-bis-3-ethylbenzthiazoline-6-sulphonic acid (ABTS) radicals as previously reported.[44] First, ABTS radicals were prepared by mixing ABTS (7 mM) and $K_2S_2O_8$ (2.45 mM) in equal volume and then stored at room temperature for 16 h. The mixture was subsequently diluted with ethanol until a light absorbance (A_{sample}) of 0.7 was obtained at 734 nm, which was monitored by a Cary 50 spectrophotometer (Varian, CA, US). DPPH radicals were prepared by dissolving DPPH in pure methanol to a concentration of

0.1 mM. To trigger the radical scavenging reactions, nanocellulose suspensions (250 mg L^{-1}) were added to the as-prepared ABTS and DPPH radicals by a 1 : 4 volumetric ratio. Reactions with ABTS and DPPH radicals took 10 and 30 min, respectively, while the DPPH reactions were kept in dark. In the end, residual ABTS and DPPH radicals were quantified by absorbance at 734 and 517 nm, respectively, and compared with a blank control using DI water to determine the scavenging activities: radical scavenging (%) = $(A_{control} - A_{sample})/A_{control} \times 100$.

Antibacterial activities of nanocelluloses were determined against Gram-positive *Staphylococcus aureus* and Gram-negative *Salmonella typhimurium*. Briefly, the bacterial strains were pre-activated by incubating bacterial stocks in Luria-Bertani (LB) media at 37 °C and 200 rpm overnight. Subsequently, the bacteria were inoculated into 5 mL of 20% LB media in a culture tube to reach 10^5–10^6 CFU mL^{-1}, and selected nanocellulose samples were added at 250 μg mL^{-1} to the cultures. The culture tubes were incubated at 37 °C and agitated at 500 rpm in an incubator shaker for 24 h, and the cell growth was determined by light absorbance at 600 nm.

3. Results and discussions

3.1. LNC extraction

A schematic production of LNCs is shown in Fig. 1. The three pretreatments were known for selective removal of hemicellulose over lignin and cellulose.[45–47] Such pulps were considered suitable for testing the performances of TEMPO-mediated oxidation reaction on lignin-rich substrates. Hemicellulose was reported to suppress the efficiency of TEMPO-mediated oxidation for nanocellulose production,[48] and hence selective removal of hemicellulose could be beneficial for LNC production. Collectively, all the three pretreatments led to the increases in cellulose and lignin contents but reduced hemicellulose contents in the pretreated pulps as compared to raw switchgrass (Table 1). Hydrothermal pretreatment at 220 °C led to complete hemicellulose removal along with 42.58% cellulose degradation, approximately twice as high as OA pretreatment, which indicated intensive polysaccharide degradation at high temperature even for a short reaction time (5 min). The mechanisms of hydrothermal pretreatment were proposed to be autohydrolysis catalyzed by hydronium ions and organic acids, respectively generated from water ionization and polysaccharides degradation at high temperature.[45,49] HT pretreatment could also form so-called pseudo-lignin when sugar degradation products recondense at high temperature under acidic condition,[49] which should be the main cause of 3.21% increase in the lignin after the pretreatment at 220 °C. When the reaction temperature of HT pretreatment was decreased to 180 °C, degradation of both cellulose and hemicellulose was mitigated, and formation of pseudo-lignin should also be avoided. DA pretreatment led to the lowest removal of cellulose and hemicellulose among the four reaction conditions. On the contrary, although catalyzed by the weak organic acid (*i.e.*, oxalic acid), OA pretreatment led to the second highest removal of cellulose and hemicellulose, and a lignin increase as high as 12.41%, suggest significant pseudo-lignin formation.[50,51] As the chemistry of pseudo-lignin is similar with genuine lignin and their characterization and separation were not comprehensively established,[49] pseudo-lignin was not specifically distinguished from genuine lignin in LNCs production in the present work.

In TEMPO-oxidized LNCs, the lignin contents were reduced compared to respective pulps, but still accounted for 16.56–27.21% of LNCs. Lignin loss caused by TEMPO-mediated oxidation ranged from 51.29–67.84%, which could be attributed to the delignification effects of oxidant NaClO,[52] as reflected by lightened colors during TEMPO oxidation (Fig. 2a). TEMPO oxidation also caused further hemicellulose removal of 55.26–59.29%.[52] The physical removal of large particles by screen was considered another cause for mass loss of all the components in the LNCs and particularly the main reason for cellulose loss as TEMPO does not degrade cellulose significantly.[17] For HT220-LNC, the cellulose loss was significantly lower than the other three samples due to a smaller amount of large particles being screened out. Switchgrass experienced more cellulose loss under the hydrothermal conditions at 220 °C, as discussed above, and the resulting pulp became finer

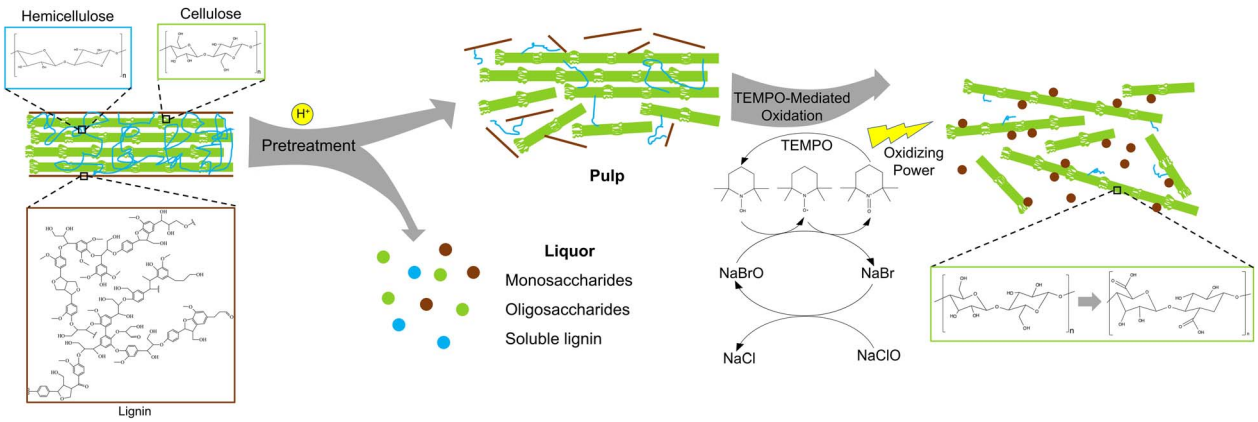

Fig. 1 Schematic production of lignin-containing nanocelluloses from raw biomass.

Table 1 Main compositions of raw switchgrass, pulps, and lignin-containing nanocelluloses

	Compositions (%)				Mass loss (%)		
	Cellulose	Xylan	Lignin	Solid recovery%	Cellulose	Xylan	Lignin
Raw SG	37.57 ± 1.91	23.33 ± 0.32	20.39 ± 0.34	—	—	—	—
HT220	46.90[a] ± 1.73	0[a]	45.76[a] ±1.96	46.0 ± 8.5	42.58 ± 8.5	100.00	−3.21[e] ± 4.41
HT180	56.89[b] ± 0.27	9.36[b] ± 0.11	27.63[b] ± 0.51	56.3 ± 1.1	14.76 ± 0.41	77.42 ± 0.27	23.72 ± 1.40
DA	50.96[c] ± 0.72	13.17[c] ± 0.07	27.99[b] ± 1.18	64.2 ± 2.6	12.92 ± 1.23	63.75 ± 0.18	11.90 ± 3.70
OA	47.34[a,c] ± 0.58	4.45[d] ± 0.05	36.80[c] ± 0.63	62.3 ± 2.3	21.50 ± 0.96	88.13 ± 0.14	−12.41[e] ± 1.92
HT220-LNC	56.02[a] ± 2.20	0[a]	27.21[a] ± 1.95	81.9 ± 0.3	2.13 ± 3.85	—	51.29 ± 3.49
HT180-LNC	46.62[a] ± 0.59	5.68[b] ± 0.04	19.48[a] ± 0.36	67.1 ± 1.3	45.03 ± 0.69	59.29 ± 0.29	52.71 ± 0.87
DA-LNC	34.31[b] ± 0.42	9.39[c] ± 0.04	16.56[a] ± 1.68	61.4 ± 0.8	58.68 ± 0.50	56.26 ± 0.17	63.68 ± 3.69
OA-LNC	49.70[a] ± 2.98	3.76[d] ± 0.25	22.38[a] ± 0.86	52.9 ± 0.7	44.48 ± 3.33	55.26 ± 3.03	67.84 ± 1.23

[a] Statistically significant from b–d. [b] Statistically significant from a, c and d. [c] Statistically significant from a, b and d. [d] Statistically significant from a–c. [e] Possible formation of pseudo-lignin.

with lesser formation of large particles. The LNCs had 34.3–56.02% cellulose contents and the CNF had 65.57%, as determined by HPLC based on two-step acid hydrolysis described above. It should be noted that there is some limitation in HPLC quantification for TEMPO-oxidized cellulose products as TEMPO-mediated oxidation could lead to the formation of polyglucuronic acid and its oligomers and/or glucose derivatives such as glucuronic acid,[53–55] which cannot be either detected or distinguished from glucose by HPLC. Thus, it can be inferred that the actual contents of cellulose-based components in the LNCs and CNF could be higher than the reported cellulose contents.

3.2. Characterizations of LNCs

The morphology of the LNCs inspected by AFM and their size distributions are shown in Fig. 3. Nanocellulose in typical fiber-shaped morphology was observed. Size distribution measured the average heights (corresponding to fiber diameters) from 1.9 to 3.2 nm and the average lengths from 541.5 to 791.4 nm, giving the highest aspect ratio of 416.5 in HT180-LNC and the

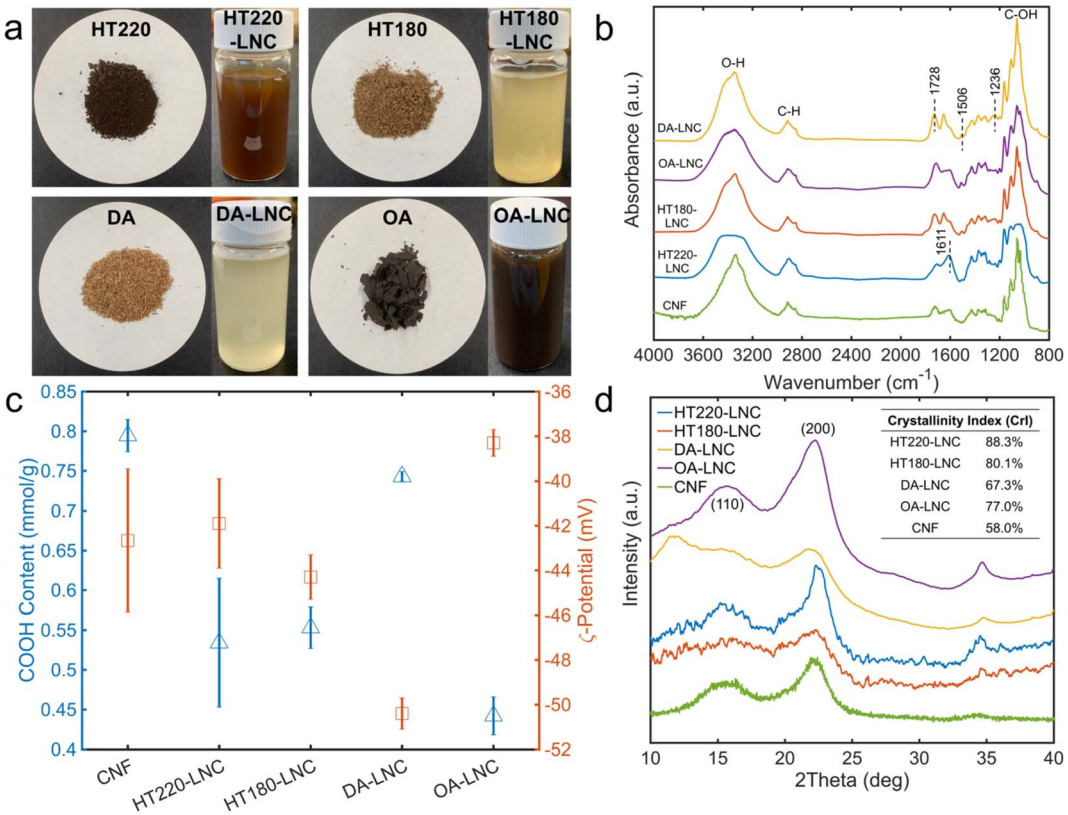

Fig. 2 Properties of LNCs. (a) Photos of the pulps and LNCs. (b) FTIR spectra. (c) Carboxyl content and ζ-potential. (d) XRD patterns, with the inset showing the crystallinity indices of LNCs and CNF.

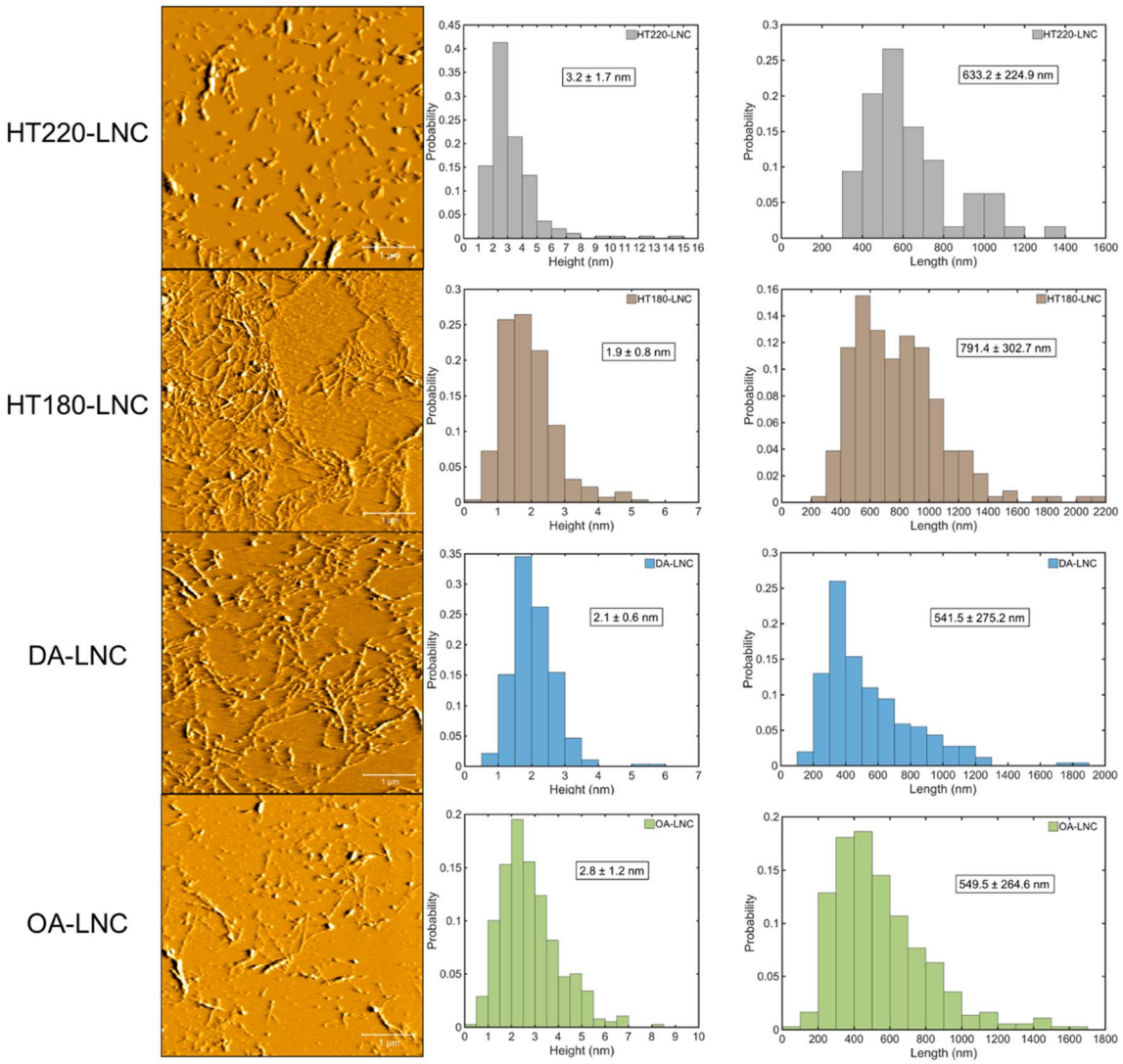

Fig. 3 Morphology and size distributions of LNCs by AFM.

lowest value of around 197 in both HT220-LNC and OA-LNC. To show the significance of size differences, a single factor analysis of variance (ANOVA) was conducted pairwise between the LNC samples. Except the lengths of DA-LNC and OA-LNC, all the average size differed significantly (p-value < 0.05) among the LNC samples. The sizes of LNCs were also analyzed by dynamic light scattering (DLS) (Fig. S1†). DLS measured the average hydrodynamic sizes of the LNCs in suspensions, but did not distinguish the radial and longitudinal dimensions, hence its results were different from those from AFM. Overall, the DLS sizes of all nanocelluloses dropped between 161 and 307 nm, among which CNF was smaller than LNC samples. Based on the compositions of LNCs, residual lignin possibly increased the diameter of nanocelluloses. In the AFM images, some nanocelluloses were coated with a sheath presumably most comprising lignin, which were more frequently observed in HT220-LNC and OA-LNC and potentially increased their fiber diameters. Meanwhile, residual lignin also appeared as near-sphere nanoparticles across all the LNC samples, but that fraction of lignin did not affect the size measurement of LNCs as they were distinguished from the fiber-shaped nanocelluloses.

The chemical structures of LNCs were further characterized by FTIR (Fig. 2b). Characteristic absorbance peaks for O–H stretching, C–H stretching, and C–OH stretching were observed at 3367, 2916, and 1061 cm^{-1}, respectively, which could indistinguishably relate with cellulose, hemicellulose, and lignin components.[56] Residual lignin was identified by peaks at 1236 cm^{-1} for syringyl ring vibration, 1506 cm^{-1} for aromatic skeletal vibration, and 1611 cm^{-1} for C=C aromatic ring vibration.[56,57] Specifically, the 1236 cm^{-1} peak was suppressed in HT220-LNC and OA-LNC, while the 1611 cm^{-1} peak increased in the same two samples, implying potential structural changes of lignin during these two pretreatments. Meanwhile, the peak at 1728 cm^{-1} related to unconjugated C=O in both hemicellulose and the carboxyl groups grafted by TEMPO oxidation.[58,59] The carboxyl contents in the LNCs were quantitatively determined by conductometric titration (Fig. 2c). Among all the samples,

lignin-free CNFs had the highest carboxyl content of 0.795 mmol g^{-1}, and DA-LNC had the highest carboxyl content of 0.743 mmol g^{-1} among the LNC samples whereas OA-LNC had the lowest (0.442 mmol g^{-1}). Carboxyl contents of the LNCs showed a direct correlation to their ζ-potentials (Fig. 2c), indicating good stabilities of the LNCs suspensions due to negative charges of carboxyl groups. On the other hand, although the lignin-free CNF possessed the highest amount of carboxyl group, its ζ-potential appeared in the middle among all the samples, which implied that residual lignin could play a beneficial role in surface charge and stability of nanocellulose.

Crystallinity of LNCs was characterized by XRD (Fig. 2d). Two characteristic peaks at around 15.7° and 22.6° were observed in all the LNCs samples, representing the (110) and (200) lattice planes of cellulose crystals, respectively.[60] HT220-LNC showed the highest crystallinity, which should be attributed to strong degradation of amorphous regions in its lignocellulosic matrix during the pretreatment. On the other hand, residual lignin seemed to not affect cellulose crystallinity as all the nanocellulose samples had relatively high lignin contents (Table 1), with HT220-LNC having the highest level.

Thermogravimetric analysis (TGA) assessed the thermostability of different nanocelluloses by inspecting their weight losses alongside temperature increase (Fig. S2†). All nanocellulose samples roughly followed a three-stage pattern in their weight losses: (1) a sharp drop started at 220–250 °C and ended by around 345 °C; (2) a transition stage which gradually dropped between 345 °C and 450 °C; and (3) another sharp drop started from 450 °C and reached a plateau at high temperature. The three-stage weight decreases related with the chemical changes of organic components in the nanocelluloses, such as degradation, dehydration and carbonization, which occurred at different temperatures until all organic components converted to carbon dioxide and water vapor and only ashes and chars remained. Meanwhile, HT220-LNC and DA-LNC exhibited some differences from other samples in their weight-loss pattern. In HT220-LNC, the transition stage (stage 2) was unobvious and merged into stage 3, showing a steady decreasing slope through 345 to 550 °C. This might be an implication of extra structural changes of the pretreated pulp through hydrothermal reactions under a severer condition. Similarly, DA-LNC did not show obvious transition from stage 2 to 3, whereas its weight loss was slower than the other samples plus a notably higher burn-off point at 715 °C. A possible explanation was the sulfonate groups introduced by sulfuric acid during DA pretreatment, which could trigger carbohydrate dehydration and char formation.[61]

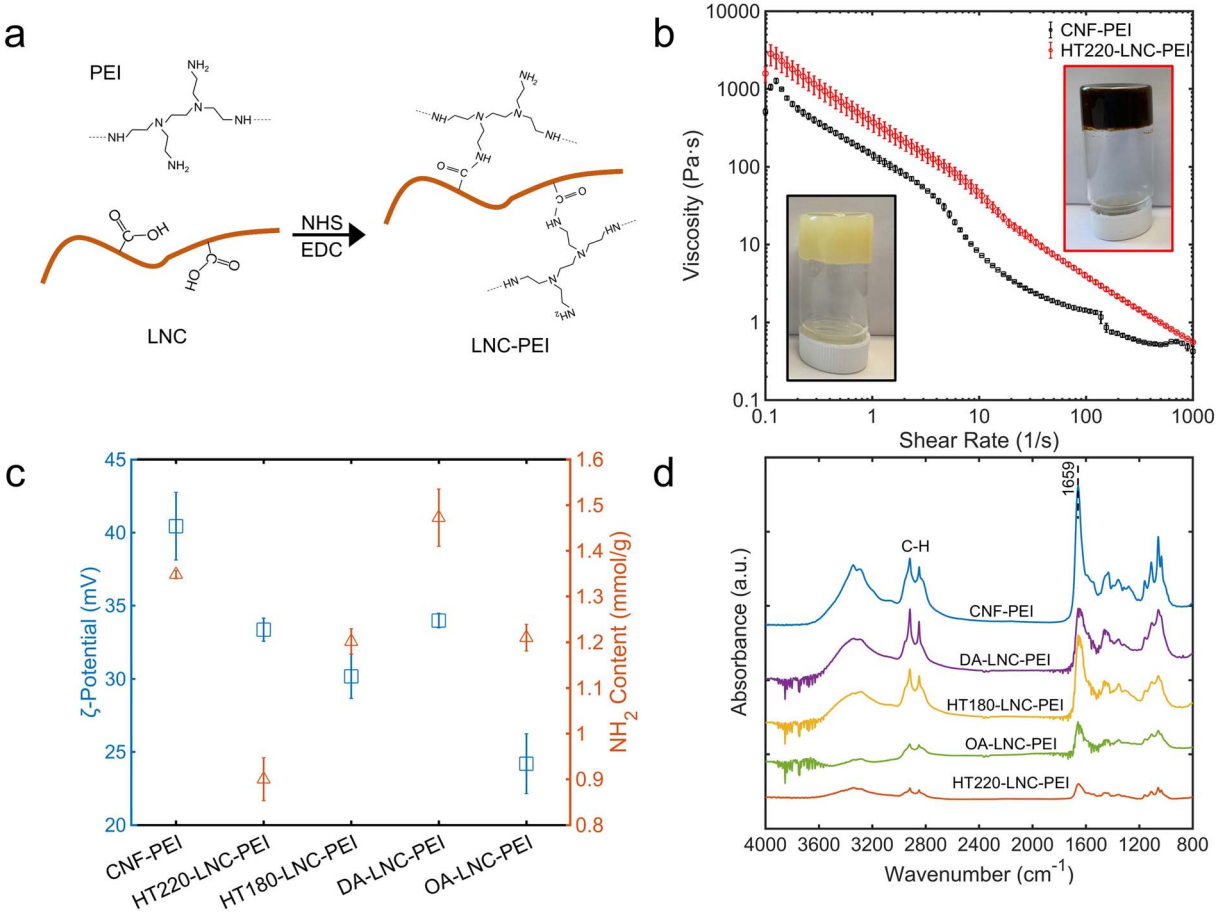

Fig. 4 Properties of PEI-modified LNCs. (a) Schematic mechanism of PEI modification of LNCs. (b) Photos and rheological properties. (c) ζ-Potential and primary amino ($-NH_2$) content. (d) FTIR spectra.

3.3. PEI modification of LNCs

Branched PEI was grafted onto LNCs *via* the reaction between the carboxyl groups on nanocelluloses and the primary amines in PEI catalyzed by EDC and NHS (Fig. 4a). The PEI-modified nanocelluloses were enriched with amino groups on their surfaces, which was characterized by FTIR, ζ-potential, and colorimetric quantification using 4-nitrobenzaldehyde (Fig. 4c and d). In FTIR, a strong peak at 1659 cm^{-1} was observed through all the PEI-modified nanocelluloses, indicating the carbonyl group (C=O) in the amide groups.[9] Compared with unmodified nanocelluloses (Fig. 2b), the C=O peaks all shifted from 1728 cm^{-1} to 1659 cm^{-1}, providing a strong evidence that the chemical changes occurred on the carboxyl groups of the nanocelluloses and amide groups were formed. Meanwhile, the C–H stretching at 2918 and 2848 cm^{-1} was intensified compared with unmodified nanocelluloses, likely from the $–CH_2–CH_2–$ bonds in PEI.[62] Another evidence for successful PEI-modification was the positive charges on the nanocelluloses. In Fig. 4c, ζ-potential of all the nanocelluloses turned positive after PEI-modification, which was attributed to the protonation of their enriched primary amino groups.[63] The contents of primary amino groups were determined based on their selective reaction with the aldehyde group in 4-nitrobenzaldehyde (Fig. 4c). The PEI-modified nanocelluloses had 0.900 to 1.473 mmol g^{-1} primary amino groups, indicating successful grafting of PEI on the nanocelluloses. On the other hand, the NH_2 content did not follow a strict correlation with ζ-potential. For instance, CNF-PEI had the highest ζ-potential whereas its NH_2 content (1.348 mmol g^{-1}) was lower than that of DA-LNC-PEI (1.473 mmol g^{-1}). Plausibly, not only primary but secondary and tertiary amino groups could also be protonated and generate positive surface charges, while 4-nitrobenzaldehyde mainly reacted and quantified primary amino groups.[43] It also suggested secondary and tertiary amino groups of PEI participate in surface modification depending on nanocellulose samples.

The hydrogels of CNF-PEI and HT220-LNC-PEI were prepared *via* a solvent evaporation process (Fig. 4b). Rheological analysis showed typical shear-thinning behavior of both hydrogels as shear rate increased. Compared with lignin-free CNF-PEI, high lignin-containing HT220-LNC-PEI showed slightly higher viscosity at the same consistency (12 wt%), and its slope of viscosity decrease remained more stable under high shear stress. The latter observation could imply lesser homogeneity of the hydrogel network of CNF-PEI, potentially due to the coagulation of nanocelluloses upon solvent evaporation, whereas such effect was suppressed in HT220-LNC-PEI due to the presence of lignin. In the SEM images (Fig. 5), both CNF- and HT220-LNC-PEI showed typical porous microstructures of nanocellulose gels. However, CNF-PEI formed thick network structures with macropores of approximately hundreds of microns in scale, while HT220-LNC-PEI showed flake-like structures with mesopores of scales smaller than those in CNF-PEI by one or two orders of magnitude. Such observation at microscale provided another evidence of the anti-coagulating effect of lignin during nanocellulose gelation. Studies of other lignin-containing nanocelluloses also reported similar anti-coagulating effects of residual lignin due to its interference with the hydrogen-bonding between nanocelluloses.[64] In addition, our findings also proved such effects were also shown in PEI-modified nanocelluloses, which can contribute to the stability of their gel structures.

We further investigated antioxidant and antimicrobial properties of PEI-modified LNCs. In Fig. 6a, the scavenging of ABTS and DPPH radicals by PEI-modified nanocelluloses were determined. At 50 mg L^{-1} unmodified lignin-free CNF did not exhibit any scavenging activities against both radicals, while the high lignin-containing HT220-LNC inactivated ABTS and DPPH by 46.33% and 13.5%, respectively, demonstrating the antioxidant properties of lignin content. The PEI-modified CNFs and LNCs showed comparable radical scavenging activities (p-value > 0.05), 94.25–100%, and 18.59–25.10% against ABTS and DPPH radicals, respectively, which were significantly higher than the unmodified CNF and HT220-LNC (p-value < 0.05). Compared with pure PEI which deactivated 12.2% DPPH radical, PEI-modified nanocelluloses exhibited higher antioxidant

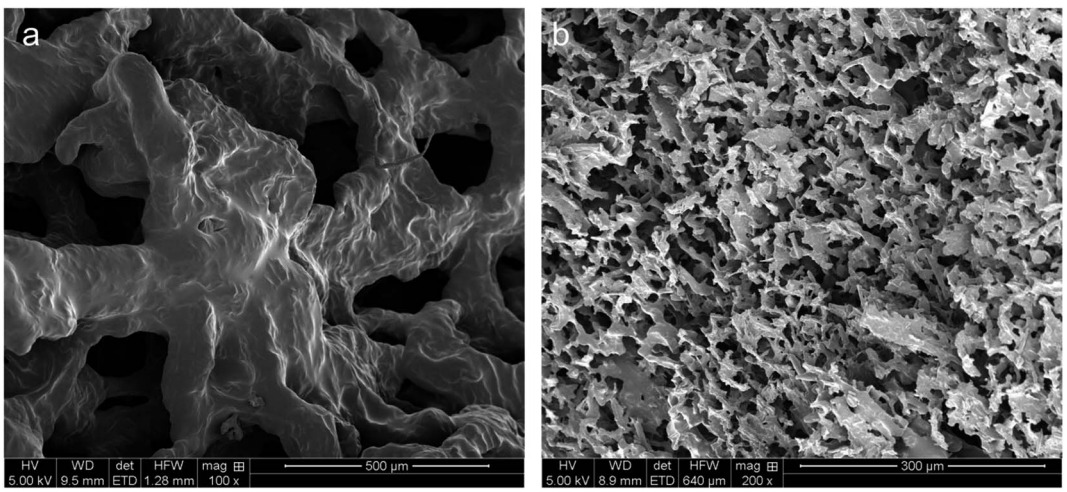

Fig. 5 SEM images of the cross sections of freeze-dried (a) CNF-PEI gel and (b) HT220-LNC-PEI gel.

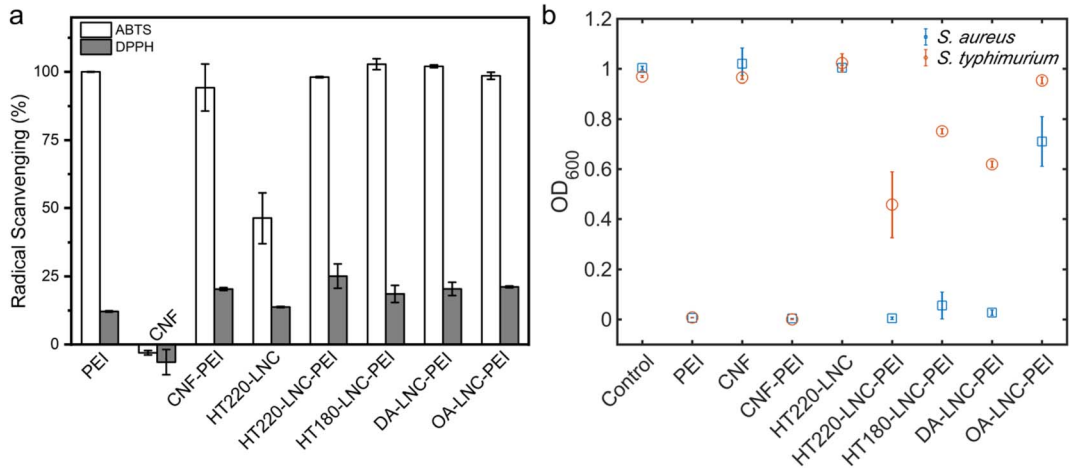

Fig. 6 Antioxidant and antibacterial activities of PEI-modified LNCs. (a) Radical scavenging activities. (b) Bacterial growth in response to the treatment of different nanocellulose samples.

activities, which could imply synergistic effects between PEI and nanocelluloses. Furthermore, residual lignin in the LNC would promote the antioxidant activities of PEI-modified nanocelluloses.

The antibacterial activities of PEI-modified nanocelluloses were assessed against a Gram-positive strain and Gram-negative strain, *i.e.*, *S. aureus* (Gram-positive) and *S. typhimurium* (Gram-negative), by monitoring their growths with the presence of nanocelluloses (Fig. 6b). After 24 h, the light absorbance at 600 nm indicated comparable growth levels of blank control and unmodified CNF and HT220-LNC in which no antibacterial activities were detected in unmodified nanocelluloses regardless of lignin content. Among the PEI-modified nanocelluloses at 250 μg mL^{-1}, all except OA-LNC-PEI achieved a near-complete inhibition of growth of *S. aureus*. For *S. typhimurium*, only CNF-PEI exhibited a complete inhibition while the PEI-modified LNCs except OA-LNC-PEI led to modest inhibition. As the positive control, pure PEI (250 μg mL^{-1}) completely inhibited the growth of both bacterial species. The antibacterial activities of PEI are attributed to its electrostatic interactions with negatively charged bacterial cell membranes, while its different efficacies against Gram-positive *vs.* Gram-negative species should be associated with the differences in their intrinsic cell membrane structures.[65] PEI content could be one cause for the different performances of PEI-modified CNF/LNCs against *S. typhimurium*, while the effects of lignin content were not clear.

Collectively, although PEI was the main source of the antioxidant and antibacterial activities of PEI-modified nanocelluloses at comparable concentrations, PEI-nanocelluloses could still be favorable in multiple aspects. First, the modification grafted PEI onto nanocellulose and could avoid contamination caused by dissolved PEI.[33,34] Moreover, nanocelluloses are known building blocks of wrapping, coating, and surfaces.[33,66] Furthermore, although PEI-modified nanocelluloses showed comparable performances at similar concentrations with pure PEI, the actual PEI contents in the PEI-nanocellulose composites should be lower, which implies improved effectiveness of PEI-modified nanocelluloses.

4. Conclusions

Lignin-containing nanocelluloses (LNCs) were efficiently extracted from switchgrass pulp *via* TEMPO-mediated oxidation. Three acid-catalyzed pretreatments, including hydrothermal, dilute acid, and choline chloride: oxalic acid, were adopted to prepare the pulp for LNCs extraction. The lignin-containing pulps yielded more than 40% LNCs. Like lignin-free nanocellulose, TEMPO grafted carboxyl groups onto the surface of LNCs and endowed them with good dispersing stability. With PEI modifications, LNCs gained additional functions including positive surface charges, antioxidant and antibacterial activities, and their lignin contents did not show negative effects against those functions but increased the hydrogel stability due to anti-coagulating. This study demonstrated that TEMPO-mediated oxidation worked efficiently on the pulps with high lignin contents, which helped improve the understanding of chemical production and modification of LNCs.

Conflicts of interest

The authors declare that they have no competing interests.

Acknowledgements

The work was in part supported by USDA National Institute of Food and Agriculture (Award No. 2021-67021-34504).

References

1 K. Pabortsava and R. S. Lampitt, *Nat. Commun.*, 2020, **11**, 4073.

2 Y. L. Zhang, S. C. Kang, S. Allen, D. Allen, T. G. Gao and M. Sillanpaa, *Earth-Sci. Rev.*, 2020, **203**, 103118.
3 J. J. Guo, X. P. Huang, L. Xiang, Y. Z. Wang, Y. W. Li, H. Li, Q. Y. Cai, C. H. Mo and M. H. Wong, *Environ. Int.*, 2020, **137**, 105263.
4 C. Jiménez-Saelices, B. Seantier, Y. Grohens and I. Capron, *ACS Appl. Mater. Interfaces*, 2018, **10**, 16193–16202.
5 F. Jiang and Y.-L. Hsieh, *J. Mater. Chem. A*, 2014, **2**, 350–359.
6 K. M. O. Håkansson, A. B. Fall, F. Lundell, S. Yu, C. Krywka, S. V. Roth, G. Santoro, M. Kvick, L. Prahl Wittberg, L. Wågberg and L. D. Söderberg, *Nat. Commun.*, 2014, **5**, 4018.
7 N. T. Cervin, E. Johansson, P. A. Larsson and L. Wågberg, *ACS Appl. Mater. Interfaces*, 2016, **8**, 11682–11689.
8 L. Bai, X. Jiang, Z. Sun, Z. Pei, A. Ma, W. Wang, H. Chen, H. Yang, L. Yang and D. Wei, *Cellulose*, 2019, **26**, 5305–5319.
9 C. Liu, R.-N. Jin, X.-k. Ouyang and Y.-G. Wang, *Appl. Surf. Sci.*, 2017, **408**, 77–87.
10 X. He, L. Liu, H. Han, W. Shi, W. Yang and X. Lu, *Macromolecules*, 2019, **52**, 72–80.
11 M. Kaushik and A. Moores, *Green Chem.*, 2016, **18**, 622–637.
12 K. Löbmann, J. Wohlert, A. Müllertz, L. Wågberg and A. Svagan, *Adv. Mater. Interfaces*, 2017, **4**, 1600655.
13 Z. Zhang, R. Liu, H. Zepeda, L. Zeng, J. Qiu and S. Wang, *ACS Appl. Polym. Mater.*, 2019, **1**, 2023–2032.
14 S. A. A. Ghavimi, E. S. Lungren, J. L. Stromsdorfer, B. T. Darkow, J. A. Nguyen, Y. Sun, F. M. Pfieffer, C. L. Goldstein, C. Wan and B. D. Ulery, *AAPS J.*, 2019, **21**, 41.
15 S. A. A. Ghavimi, E. S. Lungren, T. J. Faulkner, M. A. Josselet, Y. Wu, Y. Sun, F. M. Pfeiffer, C. L. Goldstein, C. Wan and B. D. Ulery, *Int. J. Biol. Macromol.*, 2019, **130**, 88–98.
16 M. S. Islam, L. Chen, J. Sisler and K. C. Tam, *J. Mater. Chem. B*, 2018, **6**, 864–883.
17 A. Isogai, T. Saito and H. Fukuzumi, *Nanoscale*, 2011, **3**, 71–85.
18 M. Visanko, J. A. Sirviö, P. Piltonen, R. Sliz, H. Liimatainen and M. Illikainen, *Cellulose*, 2017, **24**, 4173–4187.
19 H. Zhu, W. Luo, P. N. Ciesielski, Z. Fang, J. Y. Zhu, G. Henriksson, M. E. Himmel and L. Hu, *Chem. Rev.*, 2016, **116**, 9305–9374.
20 W. Schutyser, T. Renders, S. Van den Bosch, S. F. Koelewijn, G. T. Beckham and B. F. Sels, *Chem. Soc. Rev.*, 2018, **47**, 852–908.
21 A. Barhoum, J. Jeevanandam, A. Rastogi, P. Samyn, Y. Boluk, A. Dufresne, M. K. Danquah and M. Bechelany, *Nanoscale*, 2020, **12**, 22845–22890.
22 I. Solala, M. C. Iglesias and M. S. Peresin, *Cellulose*, 2020, **27**, 1853–1877.
23 J. A. Sirviö, M. Y. Ismail, K. Zhang, M. V. Tejesvi and A. Ämmälä, *J. Mater. Chem. A*, 2020, **8**, 7935–7946.
24 S. S. Nair, H. Chen, Y. Peng, Y. Huang and N. Yan, *ACS Sustainable Chem. Eng.*, 2018, **6**, 10058–10068.
25 C. Cai, K. Hirth, R. Gleisner, H. Lou, X. Qiu and J. Y. Zhu, *Green Chem.*, 2020, **22**, 1605–1617.
26 M. Cheng, Z. Qin, J. Hu, Q. Liu, T. Wei, W. Li, Y. Ling and B. Liu, *Carbohydr. Polym.*, 2020, **231**, 115701.
27 S. Guha, J. Ghimire, E. Wu and W. C. Wimley, *Chem. Rev.*, 2019, **119**, 6040–6085.
28 Y. Ye, Y. Zhang, Y. Chen, X. Han and F. Jiang, *Adv. Funct. Mater.*, 2020, 2003430.
29 F. Zhang, H. Ren, J. Dou, G. Tong and Y. Deng, *Sci. Rep.*, 2017, **7**, 40096.
30 Y. Wen, Z. Yuan, X. Liu, J. Qu, S. Yang, A. Wang, C. Wang, B. Wei, J. Xu and Y. Ni, *ACS Sustainable Chem. Eng.*, 2019, **7**, 6131–6139.
31 Y. Yin, X. Li, H. Ma, J. Zhang, D. Yu, R. Zhao, S. Yu, G. Nie and H. Wang, *Nano Lett.*, 2021, **21**, 2224–2231.
32 P. Vicennati, A. Giuliano, G. Ortaggi and A. Masotti, *Curr. Med. Chem.*, 2008, **15**, 2826–2839.
33 M. Wu, J. Yang, S. Chen, P. Lu and R. Wang, *Carbohydr. Polym.*, 2021, **274**, 118654.
34 M. Liu, J. Li and B. Li, *Langmuir*, 2018, **34**, 1574–1580.
35 F. Wahid, H. Bai, F.-P. Wang, Y.-Y. Xie, Y.-W. Zhang, L.-Q. Chu, S.-R. Jia and C. Zhong, *Cellulose*, 2020, **27**, 369–383.
36 M. A. Ghriga, B. Grassl, M. Gareche, M. Khodja, S. E. I. Lebouachera, N. Andreu and N. Drouiche, *Polym. Bull.*, 2019, **76**, 6001–6029.
37 Y. Okita, T. Saito and A. Isogai, *Holzforschung*, 2009, **63**, 529–535.
38 A. Sluiter, B. Hames, R. Ruiz, C. Scarlata, J. Sluiter, D. Templeton and D. Crocker, *Lab. Anal. Proced.*, 2010, **1617**, 1–16.
39 T. Saito and A. Isogai, *Biomacromolecules*, 2004, **5**, 1983–1989.
40 S. Hu, F. Jiang and Y.-L. Hsieh, *ACS Sustainable Chem. Eng.*, 2015, **3**, 2566–2574.
41 Y. Li, Q. Fu, S. Yu, M. Yan and L. Berglund, *Biomacromolecules*, 2016, **17**, 1358–1364.
42 Y. Cao and H. Tan, *Enzyme Microb. Technol.*, 2005, **36**, 314–317.
43 Y. Sun, F. Kunc, V. Balhara, B. Coleman, O. Kodra, M. Raza, M. Chen, A. Brinkmann, G. P. Lopinski and L. J. Johnston, *Nanoscale Adv.*, 2019, **1**, 1598–1607.
44 J. D. Coral Medina, A. L. Woiciechowski, A. Zandona Filho, L. Bissoqui, M. D. Noseda, L. P. de Souza Vandenberghe, S. F. Zawadzki and C. R. Soccol, *Ind. Crops Prod.*, 2016, **94**, 630–637.
45 G. Batista, R. B. A. Souza, B. Pratto, M. S. R. dos Santos-Rocha and A. J. G. Cruz, *Bioresour. Technol.*, 2019, **275**, 321–327.
46 W.-H. Chen, Y.-J. Tu and H.-K. Sheen, *Int. J. Energy Res.*, 2010, **34**, 265–274.
47 Q. Xia, C. Chen, Y. Yao, J. Li, S. He, Y. Zhou, T. Li, X. Pan, Y. Yao and L. Hu, *Nat. Sustain.*, 2021, **4**, 627–635.
48 T. Pääkkönen, K. Dimic-Misic, H. Orelma, R. Pönni, T. Vuorinen and T. Maloney, *Cellulose*, 2016, **23**, 277–293.
49 S. D. Shinde, X. Meng, R. Kumar and A. J. Ragauskas, *Green Chem.*, 2018, **20**, 2192–2205.
50 X. Li, M.-F. Li, J. Bian, B. Wang, J.-K. Xu and R.-C. Sun, *RSC Adv.*, 2015, **5**, 77147–77153.
51 H. Zhang, Y. Sun, Q. Li and C. Wan, *ACS Sustainable Chem. Eng.*, 2022, **10**, 11501–11511.

52 P. Ma, S. Fu, H. Zhai, K. Law and C. Daneault, *Bioresour. Technol.*, 2012, **118**, 607–610.
53 S. Fujisawa, T. Isogai and A. Isogai, *Cellulose*, 2010, **17**, 607–615.
54 R. Kuramae, T. Saito and A. Isogai, *React. Funct. Polym.*, 2014, **85**, 126–133.
55 R. Elboutachfaiti, C. Delattre, E. Petit and P. Michaud, *Carbohydr. Polym.*, 2011, **84**, 1–13.
56 J. Zhuang, M. Li, Y. Pu, A. J. Ragauskas and C. G. Yoo, *Appl. Sci.*, 2020, **10**, 4345.
57 J. Shi, D. Xing and J. Lia, *Energy Procedia*, 2012, **16**, 758–762.
58 Z. Tang, W. Li, X. Lin, H. Xiao, Q. Miao, L. Huang, L. Chen and H. Wu, *Polym*, 2017, **9**, 421.
59 J. I. Santos, R. Martín-Sampedro, Ú. Fillat, J. M. Oliva, M. J. Negro, M. Ballesteros, M. E. Eugenio and D. Ibarra, *Int. J. Polym. Sci.*, 2015, **2015**, 314891.
60 S. Park, J. O. Baker, M. E. Himmel, P. A. Parilla and D. K. Johnson, *Biotechnol. Biofuels*, 2010, **3**, 10.
61 F. D'Acierno, W. Y. Hamad, C. A. Michal and M. J. MacLachlan, *Biomacromolecules*, 2020, **21**, 3374–3386.
62 I. Yudovin-Farber, N. Beyth, E. I. Weiss and A. J. Domb, *J. Nanopart. Res.*, 2010, **12**, 591–603.
63 W. Yuan and H. Li, in *Nanostructures for Drug Delivery*, ed. E. Andronescu and A. M. Grumezescu, Elsevier, 2017, pp. 445–460, DOI: **10.1016/B978-0-323-46143-6.00014-2**.
64 K. Liu, H. Du, T. Zheng, W. Liu, M. Zhang, H. Liu, X. Zhang and C. Si, *Green Chem.*, 2021, **23**, 9723–9746.
65 X. Zeng, Y. Liu, Y. Xia, M. H. Uddin, D. Xia, D. T. McCarthy, A. Deletic, J. Yu and X. Zhang, *Appl. Catal., B*, 2020, **274**, 119095.
66 H. Spieser, A. Denneulin, D. Deganello, D. Gethin, R. Koppolu and J. Bras, *Carbohydr. Polym.*, 2020, **240**, 116305.